Granular segregation in circular tumblers: Theoretical model and scaling laws

Conor P. Schlick,[1] Yi Fan,[2,3] Paul B. Umbanhowar,[2] Julio M. Ottino,[2,4,5] and Richard M. Lueptow[2,5]†

[1]Department of Engineering Sciences and Applied Mathematics, Northwestern University, Evanston, IL 60208, USA

[2]Department of Mechanical Engineering, Northwestern University, Evanston, IL 60208, USA
[3]The Dow Chemical Company, Midland, MI 48667, USA
[4]Department of Chemical and Biological Engineering, Northwestern University, Evanston, IL 60208, USA
[5]The Northwestern University Institute on Complex Systems (NICO), Northwestern University, Evanston, IL 60208, USA

(Received 10 October 2014)

We model bidisperse size segregation of granular material in quasi-2D circular tumbler flow using the advection-diffusion transport equation with an additional term to account for segregation due to percolation. Segregation depends on three dimensionless parameters: the ratio of segregation to advection, Λ, the ratio of advection to diffusion, Pe, and the dimensionless flowing layer depth, ϵ. The degree of segregation in steady state depends only on the ratio of segregation effects to diffusion effects, ΛPe, and the degree of segregation increases as ΛPe is increased. The transient time to reach steady state segregation depends only on advection, which is manifested in ϵ and Pe when ΛPe is constant. This model is also applied to unsteady tumbler flow, where the rotation speed is varied with time.

1. Introduction

Segregation of dense, sheared, granular mixtures of different-sized particles occurs widely in both nature and industry. Examples include particle sorting during debris flow (Hutter *et al.* 1996) and particle separation in rotating tumbler mixers (Ottino & Khakhar 2000; Meier *et al.* 2007). In most circumstances, size segregation is undesirable and even destructive. Therefore, a model that can quantitatively predict size segregation is useful. This model should be capable of predicting two aspects of the process: i) the final particle configurations when segregation reaches steady state and ii) the transient behavior of size segregation that influences the efficiency of various industrial processes (e.g. segregation and mixing rate). While several models have been developed to predict size segregation in recent years (Shinohara *et al.* 1972; Boutreux 1998; Khakhar *et al.* 2001; Gray & Thornton 2005; Gray & Chugunov 2006; Gray *et al.* 2006; Shearer *et al.* 2008; Thornton & Gray 2008; Gray & Ancey 2009; May *et al.* 2010; Fan & Hill 2011; Fan *et al.* 2014*a*; Woodhouse *et al.* 2012; Tunuguntla *et al.* 2014), most consider less complicated granular flows, such as plug, annular shear, or chute flow. Although some of these studies (Gray & Thornton 2005; Gray *et al.* 2006; Gray & Ancey 2009; Shearer *et al.* 2008; Thornton & Gray 2008; Gray & Ancey 2009; Woodhouse *et al.* 2012) considered time-dependent segregation problems, the time-dependent segregation models in these papers were for relatively simple flows and were not compared with or validated by experiments

† Email address: r-lueptow@northwestern.edu

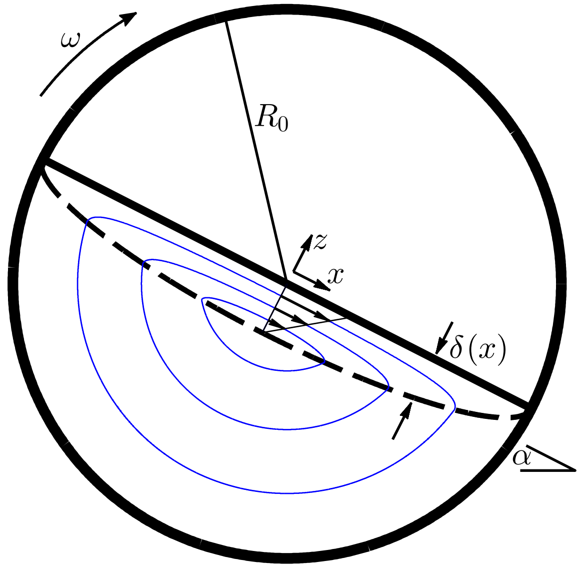

FIGURE 1. Schematic of continuous flow in a 50% full quasi-2D circular tumbler with radius R_0 rotating clockwise at angular velocity ω. Particles are in solid body rotation below the dashed curve, enter the flowing layer in the upstream (left) half of the flowing layer, flow down the flowing layer (above the dashed curve), and re-enter solid body rotation in the downstream (right) half of the flowing layer. The flowing layer has thickness $\delta(x)$ and the angle of repose is α. The x-coordinate is the streamwise direction, the y-coordinate is the spanwise direction, and the z-coordinate is normal to the free surface. The origin is located at the center of the tumbler. Streamlines for mean particle trajectories are shown as gray (blue online) curves. u and w are the velocities in the x and z directions, respectively.

or simulations. In this paper, we use rotating tumbler flow, a flow with relatively complicated kinematics, as a model flow to develop a continuum model that quantitatively predicts both steady and transient size segregation.

A schematic of continuous quasi-2D circular tumbler flow is shown in figure 1. As the tumbler rotates at angular velocity ω, most particles are in solid body rotation (below the dashed curve in figure 1) rotating with the tumbler. In the flowing layer (above the dashed curve), particles quickly flow down the slope and re-enter solid body rotation in the downstream half of the flowing layer (see the streamlines in figure 1). For a size bidisperse system, small particles (with diameter d_s) in the flowing layer fall between large particle voids, percolate downward, and enter solid body rotation towards the center of the tumbler. Large particles (with diameter d_l) segregate upward, are advected to the end of the flowing layer, and enter solid body rotation near the cylindrical tumbler wall (Williams 1968; Drahun & Bridgwater 1983; Savage & Lun 1988; Ottino & Khakhar 2000).

Various segregation patterns are observed in tumbler flow when the tumbler geometry or operating conditions are varied. For less than 50% full circular tumblers rotating with a constant angular velocity, radial segregation patterns in which small particles accumulate in the middle of the bed of particles, while large particles accumulate near the outer tumbler walls have been observed in both experiments (Cantelaube & Bideau 1995; Metcalfe 1996; Hill *et al.* 1999; Jain *et al.* 2005; Meier *et al.* 2007; Gray & Ancey 2011) and simulations (Dury & Ristow 1997, 1999; Pereira & Cleary 2013; Arntz *et al.* 2014; Alizadeh *et al.* 2014). In addition to radial segregation patterns, lobed segregation patterns are observed for circular tumblers more than 50% full (Gray & Hutter 1997; Hill *et al.* 2004; Meier *et al.* 2007, 2008), circular tumblers with a non-uniform rotation speed (Fiedor & Ottino 2005), and in steadily rotating non-circular tumblers (Hill *et al.* 1999; Ottino & Khakhar 2000; Cisar *et al.* 2006; Meier *et al.* 2006, 2007).

To model the segregation patterns observed in experiments and computational simulations, several theoretical approaches have been developed. Poincaré sections have long been used to explain the segregation patterns that occur in tumbler flows (Hill *et al.* 1999; Cisar *et al.* 2006; Meier *et al.* 2007; Christov *et al.* 2010). Cisar *et al.* (2006) developed a Lagrangian segregation model that incorporated the mean velocity of small and large particles, as well as a segregation velocity and a Langevin term to represent diffusion. From an Eulerian point of view, strange eigenmodes have been used to combine advection and diffusion to explain segregation patterns in non-circular tumblers (Christov *et al.* 2011). While results from these studies qualitatively matched experiments and DEM simulations, the methods used in them alone cannot predict the segregation patterns and the degree of segregation based on the particle sizes, the rotation speed, and the tumbler radius.

Several continuum models have been proposed for size segregation in tumblers (Prigozhin & Kalman 1998; Chakraborty *et al.* 2000; Khakhar *et al.* 2001). However, these approaches have major shortcomings, such as assuming the flowing layer depth to be infinitely thin (Prigozhin & Kalman 1998), completely separating the small particles and large particles (Khakhar *et al.* 2001), and assuming large and small particles are approximately the same size, so the variation in small and large particle concentrations is small (Chakraborty *et al.* 2000). These assumptions oversimplify the effect of key physical properties of segregation, so that it is difficult to predict and understand segregation patterns quantitatively across a broad range of physical parameters.

In this paper, we use a continuum approach based on the generic transport equation to model bidisperse size segregation in rotating circular tumblers. This continuum model has been developed and used by several research groups (Bridgwater *et al.* 1985; Savage & Lun 1988; Dolgunin & Ukolov 1995; Gray & Thornton 2005; Gray & Chugunov 2006; Gray & Ancey 2009; May *et al.* 2010; Fan & Hill 2011; Marks *et al.* 2012) in different flow geometries and has achieved success in modelling size segregation qualitatively. Most recently, within this theoretical framework, we developed a model that considers the roles of three mechanisms: advection, shear-dependent percolation, and collisional diffusion (Fan *et al.* 2014*a*). The model predicted size bidisperse segregation in bounded heap flow quantitatively and revealed that all the three mechanisms are important when modelling size segregation in complex granular flows. Specifically, using this approach, we found that the segregation patterns in bounded heaps depend on two dimensionless parameters: a parameter related to advection and segregation, Λ, and a Péclet number, Pe, related to advection and collisional diffusion. In tumbler flow, in addition to Λ and Pe, segregation also depends on a third dimensionless parameter, ϵ, the dimensionless depth of the flowing layer. Using this continuum equation approach, we parametrically study segregation patterns in 50% full circular tumblers as a function of these three dimensionless parameters.

In contrast to quasi-2D bounded heaps (the system considered by Fan *et al.* (2014*a*)), tumbler flow presents new challenges. First, in tumbler flow, the flowing layer depth varies with streamwise position, while the flowing layer in the bounded heap is assumed to have a constant depth. Second, as the segregation pattern develops, tumbler flow is time-dependent, while in bounded heaps it is sufficient to consider steady state flow. The time-dependent model allows the study of modulated flow, where the rotation speed varies with time.

2. Modelling Tumbler flow

Here, for simplicity, we consider only half full tumblers (sketched in figure 1), but the approach can readily be applied to other fill levels. Additionally, we consider only continuously flowing material for which the surface of the flowing layer is flat (figure 1), which occurs when the Froude number, $\mathrm{Fr} = \omega^2 R_0/g$, which represents the ratio of inertial to gravitational forces, is in the range $10^{-4} < \mathrm{Fr} < 10^{-2}$ (Mellmann 2001; Meier *et al.* 2007). For Froude numbers not in this range, either avalanching, cataracting, or centrifuging occurs, and different segregation mechanisms and patterns are possible (Meier *et al.* 2007).

There have been many previous studies of flow kinematics in tumblers (Makse 1999; Orpe & Khakhar 2001; Jain *et al.* 2002; Bonamy *et al.* 2002; Alexander *et al.* 2002; Meier *et al.* 2007). The velocity field in the flowing layer can be assumed to have a constant shear rate (Jain *et al.* 2004; Meier *et al.* 2007), yielding the velocity field:

$$u(x,z) = \begin{cases} \omega\left(\dfrac{R_0^2}{\delta_0^2} - 1\right)(z + \delta(x)) & \text{if } z > -\delta(x) \\ \omega z & \text{if } z \leqslant -\delta(x), \end{cases}$$
$$w(x,z) = \begin{cases} \omega\left(1 - \dfrac{\delta_0^2}{R_0^2}\right)\dfrac{xz}{\delta(x)} & \text{if } z > -\delta(x) \\ -\omega x & \text{if } z \leqslant -\delta(x), \end{cases} \tag{2.1}$$

where R_0 is the tumbler radius, u and w are the velocity components in the streamwise (x) and normal (z), respectively, and ω is the rotation rate. $\delta(x)$ is the flowing layer thickness at streamwise location x and is defined as (Makse 1999; Meier *et al.* 2007)

$$\delta(x) = \delta_0\sqrt{1 - \left(\frac{x}{R_0}\right)^2}, \tag{2.2}$$

where δ_0 is the maximum thickness of the flowing layer. It is important to note that the velocity field given in equation (2.1) is an approximation. This is evident as there is a discontinuity at the bottom of the flowing layer ($z = -\delta(x)$). However, since the particle velocity in solid body rotation near the bottom of the flowing layer is small if δ_0/R_0 is not too large, the discontinuity is inconsequential for the purposes of this approach, and equation (2.1) well describes the velocity of particles in a tumbler.

From equation (2.1), the surface velocity is

$$u(x,0) = \omega\left(\frac{R_0^2}{\delta_0} - \delta_0\right)\sqrt{1 - \left(\frac{x}{R_0}\right)^2}. \tag{2.3}$$

The velocity field, given by equation (2.1), is determined by R_0, ω, and δ_0. While previous work (Pignatel *et al.* 2012) has extensively studied the relationship between δ_0 and the system parameters, here we measure δ_0 from discrete element method (DEM) simulations. In addition to determining δ_0, DEM simulations are used to validate our theoretical modeling.

In DEM simulations, to compute the interactions between particles, we use a linear spring-dashpot force model for normal forces and a linear spring model with Coulomb friction for tangential forces. Details and validation of the DEM model appear in Fan *et al.* (2013). In the simulations presented here, particles are mm-sized spheres with density $\rho_p = 2500$ kg/m^3 and restitution coefficient 0.8. Particle-particle and particle-wall friction coefficients are set to $\mu_p = 0.4$. The binary collision time is set to $t_c = 10^{-3}$ s for

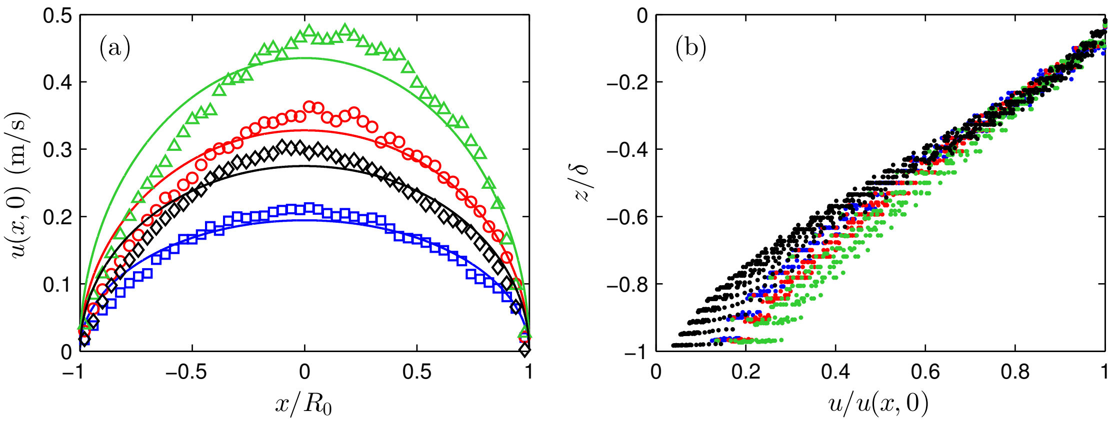

FIGURE 2. (a) Surface velocity $u(x, 0)$ vs. streamwise position x. Curves are fits of the DEM simulation data to equation (2.3). $\omega = 0.25$ rad/s, $d_s = 1$ mm, $d_l = 1.5$ mm, $\delta_0 = 7.17$ mm (dark gray, blue online, □); $\omega = 0.50$ rad/s, $d_s = 1$ mm, $d_l = 1.5$ mm, $\delta_0 = 8.47$ mm (light gray, red online, ○); $\omega = 0.75$ rad/s, $d_s = 1$ mm, $d_l = 1.5$ mm, $\delta_0 = 9.54$ mm (lighter gray, green online, △); $\omega = 0.75$ rad/s, $d_s = 1$ mm, $d_l = 3$ mm, $\delta_0 = 14.8$ mm (black, ⋄). For all datasets, $R_0 = 75$, mm and the gap between the endwalls is $4.33d_l$. (b) Streamwise velocity profile at various streamwise locations for the DEM simulations shown in (a) with corresponding colors.

greater computational efficiency, yet sufficient for modelling hard spheres (Silbert *et al.* 2007). An integration time step of $\Delta t = t_c/100 = 1 \times 10^{-5}$ s is used to assure numerical stability. To reduce particle ordering, particles of each species are given a uniform size distribution between $0.9d_i$ and $1.1d_i$, where d_i is the mean particle diameter for each species i.

The simulated tumblers have two flat, frictional endwalls separated by $4.33d_l$. The tumbler radius is $R_0 = 75$ mm, and the rotation speeds are 0.25 rad/s, 0.5 rad/s, and 0.75 rad/s. The steady state for kinematics of the mixture is assumed to occur when the dynamic angle of the repose, α, the surface velocity at the origin, and the degree of segregation no longer vary with time. Then the steady state values of kinematic variables are measured by averaging over one rotation. Figure 2 shows profiles from DEM simulations of the surface velocity in the streamwise direction and the streamwise velocity profile in the depth direction at the steady state. To determine δ_0, a nonlinear least-squares regression was implemented in MATLAB to fit the surface velocity from DEM simulations (figure 2(a)) to equation (2.3). As shown in figure 2(a), the surface velocity from the DEM simulations matches equation (2.3) reasonably well. In figure 2(b), the streamwise velocity u is plotted as a function of z for the same four DEM simulations shown in figure 2(a). The streamwise velocity decreases approximately linearly as z decreases, justifying the form of the velocity field in equation (2.1). While the streamwise velocity in the DEM simulations does not decrease to 0 at the bottom of the flowing layer as indicated by equation (2.1), it is close enough (between 5% and 20% of the surface velocity) that the velocity field given by equation (2.1) provides a reasonable approximation to the flow for use in the theoretical model. This discrepancy is likely due to the discontinuity in the streamwise velocity u in equation (2.1), as discussed previously.

3. Segregation model

To model segregation in tumbler flow, the transport equation model (Fan *et al.* 2014*a*) is applied to the flowing layer:

$$\frac{\partial c_i}{\partial t} + \nabla \cdot (\boldsymbol{u} c_i) + \frac{\partial}{\partial z}(w_{p,i} c_i) = \nabla \cdot (D \nabla c_i), \qquad x \in [-R_0, R_0],\ z \in [-\delta(x), 0]. \tag{3.1}$$

The second term on the left-hand side represents advective transport due to the mean flow of particles, while the third term represents transport normal to the free surface due to segregation (it is assumed that both species have the same velocity in the streamwise direction). The right-hand side of the equation represents collisional diffusion. In bidisperse mixtures, i refers to the small or large particles (i.e. $i = s$ or $i = l$), and no subscript is used for variables representing the combined flow. The concentration of species i is defined as $c_i = f_i/f$, where f_i is the volume fraction of species i and $f = f_s + f_l$. $\boldsymbol{u} = u\hat{\boldsymbol{x}} + v\hat{\boldsymbol{y}} + w\hat{\boldsymbol{z}}$ is the mean velocity field of the flow (both species), D is the diffusion coefficient, and $w_{p,i}$ is the percolation velocity of species i, which accounts for the relative motion of the two species in the normal direction. Below the flowing layer, particles are assumed to be in solid body rotation, so no segregation or diffusion occurs (equation (3.1) with $w_{p,i} = 0$ and $D = 0$).

The percolation velocity of each species in a bidisperse mixture can be approximated as a linear function of the shear rate and the concentration of the other species (Savage & Lun 1988; Gray & Thornton 2005; Fan *et al.* 2014*a*):

$$w_{p,s} = -S\dot{\gamma}(1 - c_s), \quad w_{p,l} = S\dot{\gamma}(1 - c_l), \tag{3.2}$$

where $\dot{\gamma}$ is the shear rate and $\dot{\gamma} = \frac{\partial u}{\partial z} + \frac{\partial w}{\partial x} \approx \frac{\partial u}{\partial z}$, since $u \gg w$ in most of the flowing layer if $R_0 \gg \delta_0$. S is the percolation length scale, which depends on the particle sizes and the particle size ratio (Fan *et al.* 2014*a*). While it would be possible to measure S directly from the tumbler simulations using the methodology described in Fan *et al.* (2014*a*) and Schlick *et al.* (2014), it would be necessary to do so during the unsteady portion of the flow when segregation is not complete. At steady state segregation, it is not possible to get a reliable value for the percolation velocity because small and large particles are almost completely separated. Since steady state segregation occurs quickly (after about 1 rotation), it is difficult to obtain a time-averaged value for the percolation velocity, and it is not possible to accurately estimate S from the tumbler simulation without running a large number of DEM simulations. In contrast, segregation occurs continuously in steady state in the flowing layer of bounded heaps (as explored in Fan *et al.* (2014*a*) and Schlick *et al.* (2014)), making it quite easy to measure the percolation velocity, and thus S, in steady state. Since the percolation velocity accounts for local particle segregation under shear, it depends only on the local kinematics. For this reason, we use the relation for S from DEM simulations of quasi-2D bounded heap flow (of mm-sized spherical glass particles) (Schlick *et al.* 2014). This further allows us to explore the general applicability of particle segregation results obtained with one flow system to segregation in another. The relation for S (Schlick *et al.* 2014) is:

$$S(d_s, d_l) = 0.26 d_s \log\left(\frac{d_l}{d_s}\right). \tag{3.3}$$

To nondimensionalize equation (3.1), lengths are scaled by R_0 and time is scaled by $1/\omega$. Dimensionless variables are denoted with a tilde. The dimensionless velocities in the flowing layer ($-\epsilon\sqrt{1-\tilde{x}^2} < \tilde{z} < 0$) are

$$\begin{aligned} \tilde{u}(\tilde{x},\tilde{z};\epsilon) &= \frac{1-\epsilon^2}{\epsilon^2}\left(\tilde{z}+\epsilon\sqrt{1-\tilde{x}^2}\right), \\ \tilde{w}(\tilde{x},\tilde{z};\epsilon) &= \frac{1-\epsilon^2}{\epsilon}\frac{\tilde{x}\tilde{z}}{\sqrt{1-\tilde{x}^2}}, \end{aligned} \tag{3.4}$$

where $\epsilon \equiv \delta_0/R_0$ is the dimensionless flowing layer depth.

Averaging over the spanwise (y) direction, neglecting diffusion in the streamwise (x) direction (as we are primarily interested in diffusion acting in opposition to segregation), assuming diffusion is constant in the flowing layer (as in Fan *et al.* (2014*a*)), and changing to dimensionless variables, equation (3.1) becomes

$$\frac{\partial c_i}{\partial \tilde{t}} + \tilde{u}\frac{\partial c_i}{\partial \tilde{x}} + \tilde{w}\frac{\partial c_i}{\partial \tilde{z}} \pm \Lambda\epsilon\frac{\partial}{\partial \tilde{z}}\left[c_i(1-c_i)\right] = \frac{\epsilon^2}{\mathrm{Pe}}\frac{\partial^2 c_i}{\partial \tilde{z}^2}, \tag{3.5}$$

where the "+" sign is taken for large particles and the "−" sign is taken for small particles. $\Lambda = S(1-\epsilon^2)/R_0\epsilon^3$ is the ratio of the advection time scale to the segregation timescale ($\Lambda = (1/\omega)/(\delta_0/w_{p,l}) = (1/\omega)/(\delta_0/S\dot{\gamma})$), and $\mathrm{Pe} = \omega R_0^2\epsilon^2/D$ is the ratio of the diffusion time scale to the advection time scale ($\mathrm{Pe} = (\delta_0^2/D)/(1/\omega)$). The numerical method used to solve this equation (with proper boundary conditions (Gray & Chugunov 2006)) is described shortly. Note that ϵ appears in equation (3.5) apart from the parameters Λ and Pe since, for the same values of Λ and Pe but different ϵ, the ratio among the three timescales remains the same, which is discussed later in this section.

The dimensionless parameters ϵ, Λ, and Pe determine the time evolution of the segregation in circular tumbler flow. Λ and Pe are functions of both control parameters (tumbler radius R_0, rotation rate ω, and small and large particle diameters d_s and d_l) and kinematic parameters (percolation length scale S, maximum flowing layer depth δ_0, and diffusion coefficient D), which can be difficult to measure. Previous results have been used to express these kinematic parameters in terms of the control parameters: S is a function of d_s and d_l only (see equation (3.3)) (Fan *et al.* 2014*a*; Schlick *et al.* 2014), D is related to the particle sizes and the shear rate (Fan *et al.* 2014*a*,*b*), and δ_0 is a function of the tumbler radius, the particle sizes, and the rotation velocity (Pignatel *et al.* 2012).

The segregation model, given by equation (3.5), has been previously applied to bounded heap flow in steady state, and good agreement between the model, DEM simulations, and experiments was observed (Fan *et al.* 2014*a*; Schlick *et al.* 2014). Tumbler flow, however, is more challenging since there is an initial transient as the initially mixed particles segregate. Moreover, the flowing layer depth for bounded heaps can be assumed to be constant, while the flowing layer depth for tumblers varies with position, further complicating the application of equation (3.5). Nevertheless, equation (3.5) can be solved to give particle concentrations at any time during the initial transient through formation of the steady state segregation pattern.

To solve equation (3.5) in the flowing layer, boundary conditions are required. At the bottom and top of the flowing layer ($z = -\delta(x), 0$), the segregation flux is equal to the diffusive flux (Gray & Chugunov 2006),

$$\pm\,\Lambda\epsilon c_i(1-c_i) = \frac{\epsilon^2}{\mathrm{Pe}}\frac{\partial c_i}{\partial \tilde{z}}. \tag{3.6}$$

The boundary condition at the bottom of the flowing layer requires that particles do not leave the flowing layer due to diffusion or segregation, but leave due to advection alone, so that the mass of each species is conserved in the entire tumbler. For more details on the validity of this boundary condition, see Fan *et al.* (2014*a*).

Equation (3.5) is solved with an operator splitting scheme (Christov *et al.* 2011; Schlick *et al.* 2013) which solves the advection step and the segregation/diffusion step separately. The advection step is solved with a matrix mapping method (Singh *et al.* 2009), and the segregation/diffusion step is solved with the implicit Crank-Nicolson method. The numerical method is detailed in our previous work (Fan *et al.* 2014*a*).

To justify including ϵ as a separate parameter in addition to Λ and Pe in equation (3.5), consider the segregation/diffusion step in the operator splitting scheme:

$$\frac{\partial c_i}{\partial \tilde{t}} \pm \Lambda\epsilon \frac{\partial}{\partial \tilde{z}}\left[c_i(1-c_i)\right] = \frac{\epsilon^2}{\mathrm{Pe}}\frac{\partial^2 c_i}{\partial \tilde{z}^2}, \tag{3.7}$$

where $-\epsilon\sqrt{1-\tilde{x}^2} < \tilde{z} < 0$. Let $\tilde{z}' = \tilde{z}/\epsilon$, so that equation (3.7) is transformed to

$$\frac{\partial c_i}{\partial \tilde{t}} \pm \Lambda \frac{\partial}{\partial \tilde{z}'}\left[c_i(1-c_i)\right] = \frac{1}{\mathrm{Pe}}\frac{\partial^2 c_i}{\partial \tilde{z}'^2}, \tag{3.8}$$

where $-\sqrt{1-\tilde{x}^2} < \tilde{z}' < 0$. Since equation (3.8) no longer depends on ϵ, it would be expected that, for Λ and Pe constant, similar segregation patterns should occur for different ϵ. Note that it is not expected that the segregation patterns (nor the time to reach steady state) should be identical, since the velocity field and the geometry of the flowing layer depend on ϵ. The effect of ϵ on segregation patterns is discussed in detail in section 5.1.

4. Model predictions

Figure 3 shows the evolution of the small particle concentration for three different values of Λ for an initially mixed ($c_s = c_l = 0.5$ everywhere), clockwise rotating tumbler with Pe $= 10$ and $\epsilon = 0.1$. In each case, the small particles fall to the bottom of the flowing layer as they move downstream in the flowing layer (left to right in figure 1), and gather in the center of the bed of particles in the tumbler; large particles rise to the top of the flowing layer as they move downstream, and accumulate near the cylindrical wall of the tumbler.

Segregation is stronger in the first column of figure 3 than in the other two columns, since Λ is larger. At 1/4 rotation, approximately half the particles have transited the flowing layer, while the other half have not. Particles that have not yet transited the flowing layer remain well-mixed, while particles that have gone through the flowing layer have begun to segregate. This is evident in a close-up of the flowing layer for this case (1st column of figure 3 after 1/4 rotation) in figure 4. Particles (which have not yet gone through the flowing layer) enter the flowing layer mixed (orange) on the left, and as they flow down the flowing layer (left to right in figure 4), they segregate.

After 1/2 rotation in the first column of figure 3, most of the particles have passed through the flowing layer once and have begun to segregate; after 1 rotation, most of the particles have passed through the flowing layer twice, and the segregation is enhanced compared to 1/2 rotation. The system has reached steady state after about 1 rotation, since there is not a large difference in the amount of segregation after 1 rotation compared to after 4 or 8 rotations. At a reduced Λ (second column of figure 3), segregation takes longer and is not as strong, and steady state requires about 4 rotations to be reached. At the smallest value of Λ (final column of figure 3), there is little segregation, except for a small core comprised of a slightly higher concentration of small particles, which appears after about 4 rotations. The steady state segregation pattern and the time it takes to achieve steady state is discussed in further detail in section 5.

To validate the theoretical model, we compare particle concentrations from theory

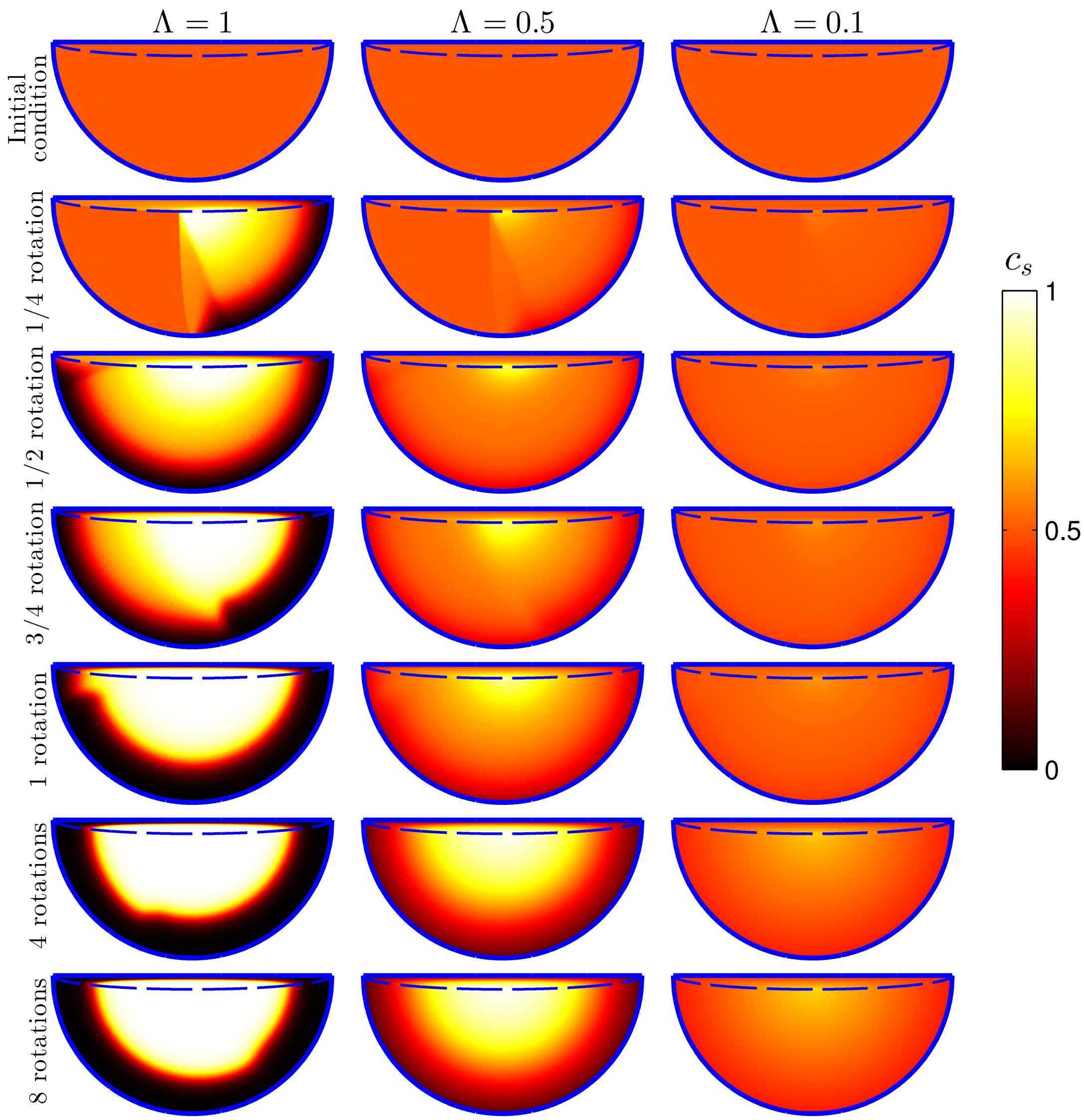

FIGURE 3. Theoretical predictions of small particle concentrations (solution to equation (3.5)) in the particle filled portion of the tumbler for three different flow and segregation conditions at various times. Dashed curves indicate the bottom of the flowing layer. Pe = 10 and $\epsilon = 0.1$.

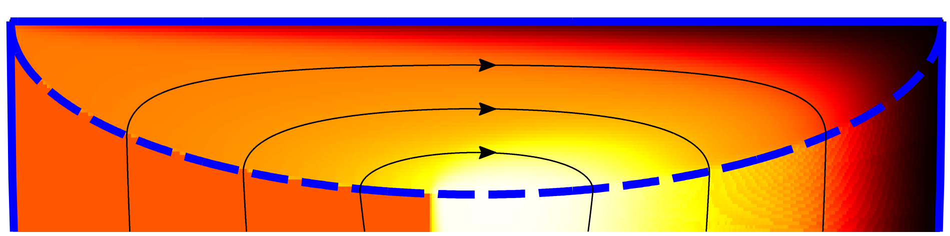

FIGURE 4. Close-up of the tumbler flowing layer after 1/4 rotation for the case shown in the first column of figure 3. Dashed curve indicates the bottom of the flowing layer. Streamlines for the mean particle flow shown as solid black curves. The colormap is the same as in figure 3.

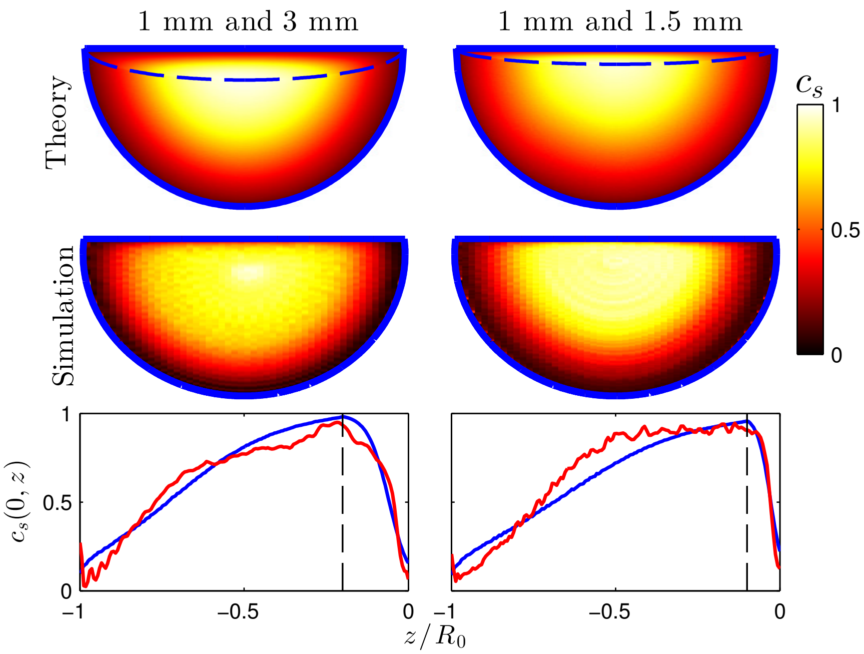

FIGURE 5. Steady state small particle concentrations in the particle filled portion of the tumbler for theory (first row) and DEM simulation (2nd row). (3rd row) Small particle concentration along a radial slice through the domain at $x = 0$ for theory (black, blue online) and simulation (gray, red online). Black dashed line represents flowing layer boundary at $z/R_0 = -\epsilon$. 1st column: $d_s = 1$ mm, $d_l = 3$ mm, $\omega = 0.75$ rad/s, $R_0 = 75$ mm, $S = 0.29$ mm, $\delta_0 = 14.78$ mm, $D = 16.1$ mm^2/s; $\epsilon = .197$, $\Lambda = 0.49$, Pe $= 10.17$. 2nd column: $d_s = 1$ mm, $d_l = 1.5$ mm, $\omega = 0.25$ rad/sec, $R_0 = 75$ mm, $S = 0.11$ mm, $\delta_0 = 7.17$ mm, $D = 5.27$ mm^2/s; $\epsilon = .096$, $\Lambda = 1.64$, Pe $= 2.46$.

and DEM simulation for 1 mm and 3 mm diameter particles and 1 mm and 1.5 mm diameter particles in a tumbler with radius $R_0 = 75$ mm and rotation rates of $\omega = 0.75$ rad/s and $\omega = 0.25$ rad/s for the two simulations respectively in figure 5. For these two flow conditions, the diffusion coefficient is calculated directly from the DEM simulation using the method described in Fan *et al.* (2014*a*), and S is determined from the particle sizes as described by Schlick *et al.* (2014). For both flow conditions, the steady state theoretical predictions qualitatively match the steady state concentrations from simulations, as shown in the first two rows of figure 5. Furthermore, the model predictions quantitatively match the DEM simulations reasonably well, as shown in the last row of figure 5 which depicts the small particle concentration along a radial slice through the domain at $x = 0$.

To compare results from the segregation model to experiments without using data from DEM simulations, it is necessary to know the flowing layer depth δ_0, the diffusion coefficient D, and the percolation length scale S. The flowing layer depth δ_0 was extracted from videos of the experiment itself and confirmed by a previous empirical relation Pignatel *et al.* (2012); the diffusion coefficient D was based on the dependence of D on the shear rate in bounded heap flow Fan *et al.* (2014*a*) using the average shear rate according to the velocity field (2.1) occurring in the tumbler; and the segregation coefficient S was based on the relation for steady segregation in bounded heap flow Fan *et al.* (2014*a*); Schlick *et al.* (2014). Thus, Λ, Pe, and ϵ are determined in terms of d_s, d_l, R_0, and ω, and the concentration evolution can be estimated based on the control parameters

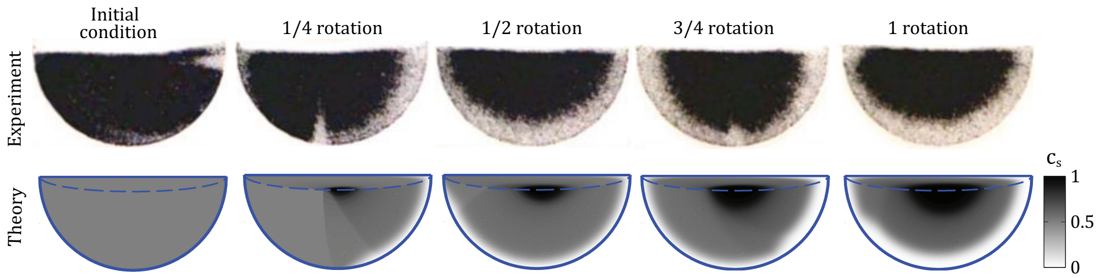

FIGURE 6. Segregation patterns in the particle filled portion of the tumbler for experiment (first row) and theory (second row). $d_s = 1$ mm (black particles), $d_l = 3$ mm (clear particles), $\omega = 0.4$ rad/s, $R_0 = 140$ mm, $S = 0.29$ mm, $\delta_0 = 21.98$ mm, $D = 2.56$ mm^2/sec; $\epsilon = .157$, $\Lambda = 0.52$, $\mathrm{Pe} = 75.49$. D and δ_0 estimated from Fan *et al.* (2014*b*) and Pignatel *et al.* (2012), respectively. The "initial condition" in the experiment is actually obtained a very short amount of time after the tumbler has begun to rotate, so the concentration discontinuity has already formed. Experimental images courtesy of Steve Meier.

only. Figure 6 compares theory to experiment for 3 mm clear and 1 mm black spherical glass beads rotated in a tumbler of radius $R_0 = 140$ mm at $\omega = 0.4$ rad/s. Note that the experiments were performed with black and clear particles in a tumbler with finite thickness. Because of the clear particles, what appears as black in the experiment is actually a mixture of clear and black particles. Thus, it is difficult to visually differentiate black and clear particles for the clear particle concentration, c_{clear}, near 0.5, as is evident in the experimental initial condition which is nearly all black for $c_{\text{clear}} = 0.5$ throughout the tumbler. Nevertheless, there is qualitative agreement between theory and experiment as a similar radial segregation pattern is observed in both. In addition, a discontinuity in the small particle concentration is observed in both experiment and theory for 1/4 and 3/4 rotation, representing the location of the initial segregation of particles when the tumbler begins to rotate. Note that there are no arbitrarily adjustable fitting parameters in the model. In fact, the velocity field and S come directly from well-established relations or previous results (for an entirely different flow field in the case of S). The similarity between the experiments and theory demonstrates the power of this segregation modelling approach.

5. A parametric study of ϵ, Λ, and Pe

Since equation (3.5) predicts segregation patterns in tumbler flow consistent with DEM simulations and experiments, it is now possible to parametrically study the effects of ϵ, Λ, and Pe. Section 5.1 explores the effect of ϵ, and section 5.2 explores the effect of Λ and Pe.

5.1. *Effect of ϵ on segregation*

The effect of the flowing layer thickness, $\epsilon = \delta_0/R_0$, on the system is shown in figure 7. For the same values of Λ and Pe, but different ϵ, the steady state segregation patterns are qualitatively similar, as predicted in section 3, since the ratio between the segregation timescale and the diffusion timescale remains constant. The quantitative difference is shown in figure 8(a), which plots the small particle concentration at $x = 0$ for the three cases shown in figure 7. The three curves match reasonably well in the fixed bed, $z/R_0 < -\epsilon$. The major difference in the concentration occurs for values of z/R_0 near 0, due to the difference in flowing layer thickness.

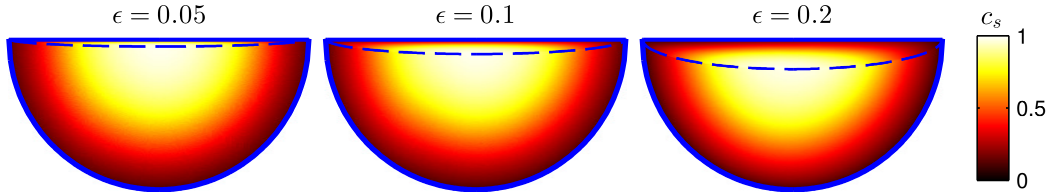

FIGURE 7. Steady state small particle concentration in the particle filled portion of the tumbler for three different values of ϵ. Dashed curves represent the bottom of the flowing layer. $\Lambda = 1$, $\mathrm{Pe} = 5$.

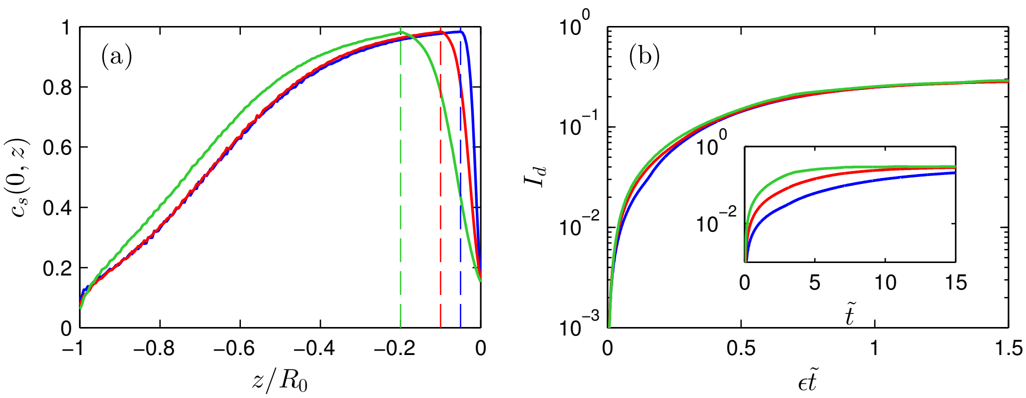

FIGURE 8. (a) Steady state small particle concentration along a radial slice at $x = 0$. Dashed lines represent the bottom of the flowing layer at $z/R_0 = -\epsilon$ for each case. (b) I_d as a function of ϵt. Inset shows I_d as a function of t. In each panel, $\epsilon = 0.05$ (black, blue online), $\epsilon = 0.1$ (dark gray, red online), and $\epsilon = 0.2$ (light gray, green online). $\Lambda = 1$, $\mathrm{Pe} = 5$.

To further assess the mixing and segregation in tumbler flow, we use the intensity of segregation (Danckwerts 1952)

$$I_d(c) = \frac{1}{\bar{c}(1-\bar{c})} \frac{\int_\Omega (c-\bar{c})^2 d\Omega}{\int_\Omega d\Omega}, \tag{5.1}$$

where Ω is the domain (particle filled portion of the tumbler) and $\bar{c} = 0.5$ is the average concentration. For a completely mixed state, $c = \bar{c}$ everywhere, and $I_d = 0$; for a completely segregated state, $c = 0$ or $c = 1$ everywhere, and $I_d = 1$. Since c is a function of time, I_d is a function of time as well.

In figure 8(b), $I_d(t)$ is plotted for the three cases shown in figure 7. $I_d = 0$ initially, and I_d increases as t increases and particles segregate more. As $t \to \infty$, I_d approaches approximately the same value (≈ 0.3) for all three cases. When time is scaled by $1/\epsilon$, all three curves collapse well. To understand this scaling, consider the surface velocity, $\tilde{u}(x, 0) \approx (1/\epsilon)\sqrt{1-\tilde{x}^2}$. As ϵ decreases, the surface velocity increases, meaning that each particle spends less time in the flowing layer, and thus has less time to diffuse and segregate. In order to reach steady state, the particles must make more passes through the flowing layer. Therefore, since the surface velocity is inversely related to ϵ, scaling time by $1/\epsilon$ effectively keeps the time each particle spends in the flowing layer the same across different values of ϵ.

5.2. *Effect of* Λ *and Pe on segregation*

The effect of Λ and Pe on segregation is revealed by multiplying each term in equation (3.5) by Pe:

$$\frac{\partial c_i}{\partial\left(\tilde{t}/\mathrm{Pe}\right)} + \mathrm{Pe}\tilde{\boldsymbol{u}}\cdot\nabla c_i \pm \Lambda\mathrm{Pe}\epsilon\frac{\partial}{\partial\tilde{z}}\left[c_i(1-c_i)\right] = \epsilon^2\frac{\partial^2 c_i}{\partial\tilde{z}^2}. \tag{5.2}$$

In this equation, time is rescaled by Pe ($\tilde{t}\to\tilde{t}/\mathrm{Pe}$ and $\tilde{\boldsymbol{u}}\to\mathrm{Pe}\tilde{\boldsymbol{u}}$). When $\epsilon\ll 1$, the velocity field in the flowing layer is $\tilde{\boldsymbol{u}}\approx(1/\epsilon^2)(\tilde{z}+\epsilon\sqrt{1-\tilde{x}^2})\hat{\boldsymbol{x}}$. At steady state, the concentration is primarily a function of z in the flowing layer, and only weakly depends on x. Therefore, since $\partial c/\partial x\approx 0$ and $w\approx 0$, $\boldsymbol{u}\cdot\nabla c\approx 0$. Thus, in steady state,

$$\pm\,\Lambda\mathrm{Pe}\frac{\partial}{\partial\tilde{z}}\left[c_i(1-c_i)\right]\approx\epsilon\frac{\partial^2 c_i}{\partial\tilde{z}^2} \tag{5.3}$$

in the entire flowing layer, and the product $\Lambda\mathrm{Pe}=S\omega R_0(1-\epsilon^2)/\epsilon D$ determines the steady state concentrations for $\epsilon\ll 1$. Physically, ΛPe represents the ratio of the diffusion timescale to the segregation timescale. If ΛPe is small, the granular mixture in the tumbler is well-mixed in steady state because diffusion dominates in the flowing layer; if ΛPe is large, segregation dominates in the flowing layer, and the granular mixture in the tumbler is segregated in steady state.

As shown in section 5.1, the steady state concentration depends weakly on ϵ provided Λ and Pe remain constant. Thus, for any ϵ, ΛPe determines the steady state concentration. Therefore, we set $\epsilon=0.1$ and examine only the effects of varying Λ and Pe in the rest of this section. Figure 9 shows steady state concentration configurations for different values of Λ and Pe. For ΛPe constant (columns), the steady state concentration contours are nearly identical for different values of Pe, as expected from equation (5.3). Furthermore, the concentrations of small particles through a radial slice (at $x=0$) in the domain are shown in the bottom row of figure 9. For ΛPe constant, particle concentrations in steady state are quantitatively similar.

To emphasize the equivalence of segregation with equal ΛPe, figure 10 shows I_d as a function of time for different values of Λ and Pe. Motivated by equation (5.2), time is rescaled by Pe, similar to figure 8(b), where time is rescaled by $1/\epsilon$. At steady state, the largest ΛPe gives the strongest segregation, and I_d is the largest in this case. In figure 10, this rescaling causes data with constant ΛPe to collapse. Thus, the value of ΛPe determines the steady state concentration configuration (and the ultimate value for I_d), and Pe (or, alternatively, Λ) determines the time to achieve steady state when ΛPe is constant.

To examine the effect of ΛPe on the segregation in tumbler flow further, figure 11 plots the steady state value of I_d as a function of ΛPe. For each value of ΛPe, six different Λ and Pe combinations are considered. For ΛPe constant, all of the different combinations of Λ and Pe give approximately the same value for I_d, as expected from figures 9 and 10. As ΛPe increases, I_d increases as a power law for $\Lambda\mathrm{Pe}<O(1)$: $I_d\sim(\Lambda\mathrm{Pe})^2$. This scaling of I_d for small values of ΛPe is investigated through an asymptotic analysis in appendix A. As ΛPe continues to increase, I_d asymptotically approaches $I_d=1$, which represents perfect segregation ($c_s=0$ or $c_s=1$ everywhere).

The steady state concentration in tumbler flow depends only on the relative strength of segregation and diffusion, determined by the parameter ΛPe, which represents the ratio of the diffusion timescale to the segregation timescale. For comparison, the steady state concentration for bounded heap flow depends on the effects of advection, as well as diffusion and segregation, as shown in Fan *et al.* (2014*a*). If advection effects are strong in bounded heaps, the inlet condition is preserved, as particles traverse the entire length

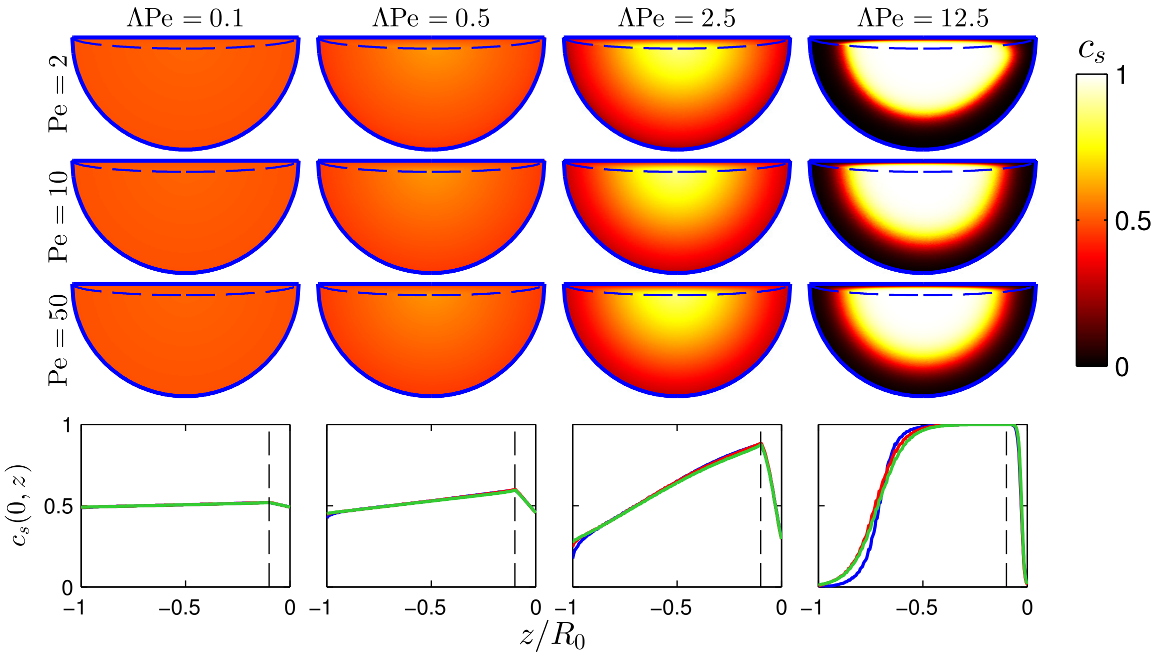

FIGURE 9. (First 3 rows) Steady state small particle concentration in the particle filled portion of the tumbler for different Λ and Pe. (Last row) Steady state small particle concentration along the radial slice $x = 0$ for constant ΛPe and Pe = 2 (black, blue online), Pe = 10 (dark grey, red online), and Pe = 50 (light gray, green online). Dashed lines indicate the flowing layer boundary ($z/R_0 = -\epsilon$). $\epsilon = 0.1$.

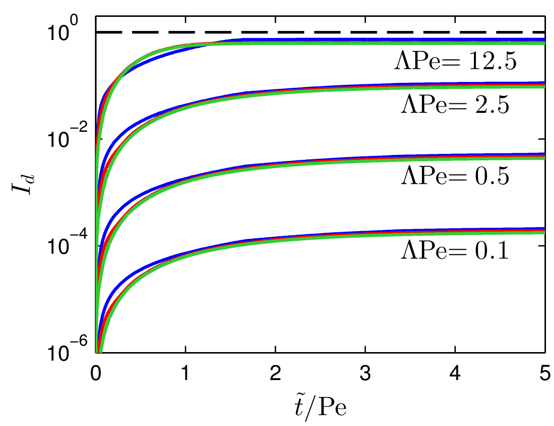

FIGURE 10. Mixing (as measured by I_d) vs. time (rescaled by Pe) for the cases in figure 9. Pe = 2 (black, blue online), Pe = 10 (dark grey, red online), and Pe = 50 (light grey, green online). $\epsilon = 0.1$.

of the flowing layer quickly with little time to diffuse or segregate. In the tumbler, if advection is strong particles do not have time to segregate or diffuse much during any single pass through the flowing layer. However, as particles pass through the flowing layer many times, steady state is ultimately reached as a result of an equilibrium between the effects of segregation and diffusion alone. Therefore, the steady state segregation pattern depends on only the product ΛPe, in contrast to bounded heaps where it depends on

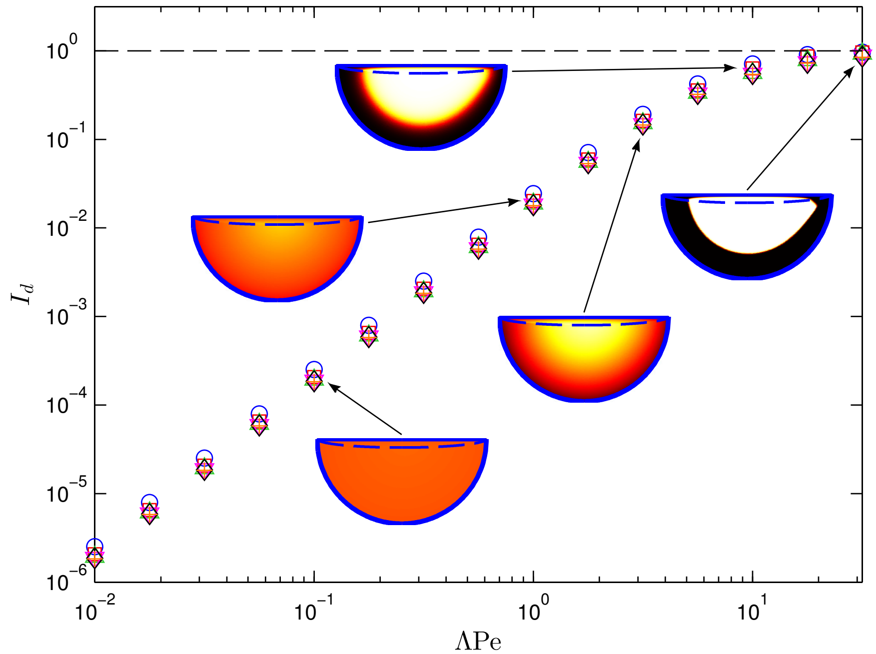

FIGURE 11. Steady state value of I_d vs. ΛPe for various combinations of Λ and Pe. Representative steady state small particle concentration contours are shown for five values of ΛPe. Pe $= 1$ ($\circ$), Pe $= 2$ ($\square$), Pe $= 5$ ($\triangle$), Pe $= 10$ ($\triangledown$), Pe $= 20$ ($\diamond$), Pe $= 50$ ($+$). $\epsilon = 0.1$.

both Λ and Pe. While ΛPe controls the steady state concentration, the time to steady state depends on ϵ and Pe, as shown in figures 8(b) and 10.

6. Modulated flow

Fiedor & Ottino (2005) experimentally studied segregation patterns for modulated flow in a tumbler by varying ω sinusoidally with time. In their study, both lobe segregation patterns and radial segregation patterns were obtained, depending on the period of the modulation of ω. If the period of the tumbler rotation (i.e. time to complete one rotation) divided by the period of the modulation is even, then lobe segregation patterns occur, and if the period of the tumbler divided by the period of the modulation is odd, then radial segregation patterns occur. To further demonstrate the capability of our approach to unsteady flow and to better understand the underlying mechanisms, we apply our model to modulated tumbler flow.

Implementing modulated flow by varying the rotation speed directly in the theory is quite difficult, because the dimensionless parameters Λ, Pe, and ϵ, and thus the velocity field $\tilde{\boldsymbol{u}}$, all vary continuously with time. However, Fiedor & Ottino (2005) postulated that lobe patterns occur due to the changing flowing layer depth. To test this hypothesis, we consider a step function for varying ϵ, while leaving Λ and Pe constant:

$$\epsilon(t) = \begin{cases} 0.1 & \text{if} \quad \mathrm{mod}\,(t, T_\omega) < T_\omega/2, \\ 0.05 & \text{if} \quad \mathrm{mod}\,(t, T_\omega) \geqslant T_\omega/2, \end{cases} \tag{6.1}$$

where $T_\omega = 2\pi/f_E$ is an integer multiple of the tumbler rotation period, and f_E is the forcing frequency of the modulation. In an experiment or DEM simulation, it would be quite difficult to vary ϵ while Λ and Pe remain constant, as each are functions of the rotation speed, the tumbler radius, and the particle diameters in nontrivial ways. However, in this section, we only seek to test the hypothesis that lobe patterns in a flow with modulated rotation speed occur due to the varying flowing layer depth, and that the other factors that come about in modulated flow (such as varying of Λ and Pe or the acceleration of particles in the flowing layer due to the change in rotation speed) play a minimal role in the final segregation pattern. Moreover, applying the segregation model to modulated flow further demonstrates the power that this approach has to unsteady flows.

Figure 12 shows small particle concentration for different values of f_E for theory (first row) and experiment (Fiedor & Ottino 2005) (second row). For the experiment and the theory, the images are obtained after a few rotations, and these patterns do not change substantially as the tumbler continues to rotate. Λ and Pe were chosen such that segregation is strong, and are not meant to exactly match the experimental conditions. The segregation patterns observed in both the theory and experiment are qualitatively similar, with lobe patterns occurring for f_E even and radial patterns occurring for f_E odd. While there is more complex structure associated with the theory compared to the experiment (probably due to the step change in ϵ rather than the smoothly varying ϵ in the experiments), the qualitative agreement between the two is remarkable given the simplicity of the underlying assumptions. Thus, this confirms the hypothesis of Fiedor & Ottino (2005) that the lobe patterns are caused by variation in the flowing layer depth.

For f_E even in figure 12, the lobe segregation patterns that occur have $f_E/2$ lobes; for f_E odd, radial segregation patterns without distinct lobes occur. For any f_E, when there is an abrupt switch from $\epsilon = 0.1$ to $\epsilon = 0.05$, the small particles at the bottom of the flowing layer when $\epsilon = 0.1$ are immediately switched to solid body rotation, creating a region in the solid body of mostly small particles. The flowing layer, at this point, is mostly large particles, and thus a region of large particles immediately follows the small particles in solid body rotation. When f_E is even, particles enter the flowing layer at approximately the same time in each cycle, and this effect is reinforced. Thus, the lobe pattern is stabilized. For f_E odd, particles enter the flowing layer half a period removed from the previous cycle, and the effect is diminished. Consequently, only radial segregation patterns occur, though there are still slight incursions of large particles into the small particle regions, consistent with the experiments.

7. Conclusion

Using the continuum transport equation model of Fan *et al.* (2014*a*) we have developed a theoretical approach for predicting granular segregation patterns in bidisperse tumbler flow. In contrast to bounded heap flow, the system studied by Fan *et al.* (2014*a*), tumbler flow offers new challenges, such as a varying flowing layer depth and an unsteady transient. Theoretical predictions are consistent with results from experiments and discrete element method simulations. The model utilizes three dimensionless parameters: a parameter related to the segregation, Λ, a Péclet number, Pe, related to collisional diffusion, and the dimensionless flowing layer depth, ϵ. Steady state particle concentrations are determined primarily by the product ΛPe and are insensitive to ϵ. However, for ΛPe constant, the time to steady state depends on ϵ and Pe. Using this model, modulation of the rotational speed of the tumbler can be simulated by varying the parameter ϵ. Both lobe and radial segregation patterns are obtained depending on the frequency of the modulation, similar to experiments (Fiedor & Ottino 2005).

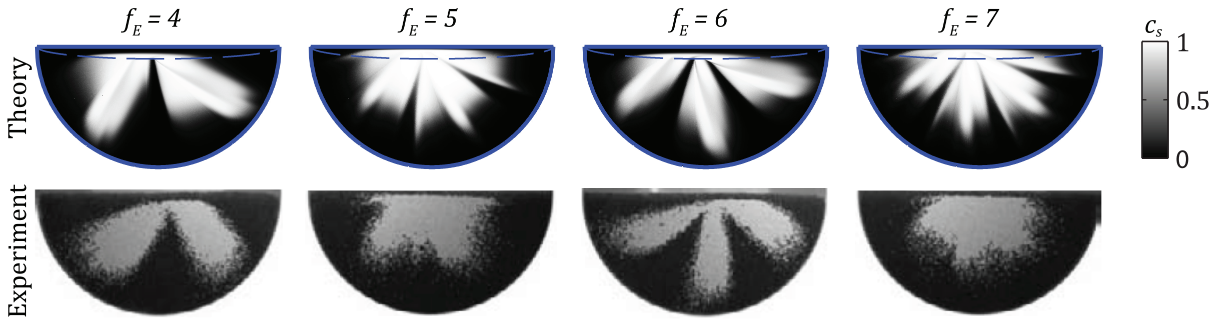

FIGURE 12. Small particle concentration in the particle-filled portion of the tumbler for modulated flow for theory (first row) and experiment (Fiedor & Ottino 2005) (second row). Modulated flow is realized by varying ϵ according to equation (6.1) for various f_E. In both theory and experiment, the volume ratio of large particles to small particles is 2:1 (in contrast to 1:1 in the rest of the paper). $\Lambda = 2$, $\mathrm{Pe} = 10$. Experimental images are from Fiedor & Ottino (2005), © 2005 Cambridge University Press, reprinted with permission.

Much work remains for modeling tumbler flows. First, it would be useful in many industrial applications to relate segregation patterns to the control parameters of the system (such as the rotation speed, the tumbler radius, and the particle sizes) instead of the dimensionless parameters (Λ, Pe, and ϵ). Additionally, while only 50% full circular tumblers were considered here, this approach can be generalized to non-half full circular tumblers, as well as tumblers with non-circular cross-sections.

This research was funded by NSF Grant CMMI-1000469 and The Dow Chemical Company. We thank Karl Jacob for a careful reading and helpful comments.

REFERENCES

Alexander, A., Shinbrot, T. & Muzzio, F. J. 2002 Scaling surface velocities in rotating cylinders as a function of vessel radius, rotation rate, and particle size. *Powder Technol.* **126** (2), 174–190.

Alizadeh, E., Bertrand, F. & Chaouki, J. 2014 Comparison of DEM results and lagrangian experimental data for the flow and mixing of granules in a rotating drum. *AIChE J.* **60** (1), 60–75.

Arntz, M. M. H. D., Beeftink, H. H., den Otter, W. K., Briels, W. J. & Boom, R. M. 2014 Segregation of granular particles by mass, radius, and density in a horizontal rotating drum. *AIChE J.* **60** (1), 50–59.

Bonamy, D., Daviaud, F. & Laurent, L. 2002 Experimental study of granular surface flows via a fast camera: A continuous description. *Phys. Fluids* **14** (5), 1666–1673.

Boutreux, T. 1998 Surface flows of granular mixtures: II. segregation with grains of different size. *Eur. Phys. J. B* **6** (3), 419–424.

Bridgwater, J., Foo, W. S. & Stephens, D. J. 1985 Particle mixing and segregation in failure zones - theory and experiment. *Powder Technol.* **41** (2), 147–158.

Cantelaube, F. & Bideau, D. 1995 Radial segregation in a 2d drum: An experimental analysis. *Europhys. Lett.* **30** (3), 133–138.

Chakraborty, S., Nott, P. R. & Prakash, J. R. 2000 Analysis of radial segregation of granular mixtures in a rotating drum. *Eur. Phys. J. E* **1** (4), 265–273.

Christov, I. C., Ottino, J. M. & Lueptow, R. M. 2010 Chaotic mixing via streamline jumping in quasi-two-dimensional tumbled granular flows. *Chaos* **20** (2).

Christov, I. C., Ottino, J. M. & Lueptow, R. M. 2011 From streamline jumping to strange eigenmodes: Bridging the lagrangian and eulerian pictures of the kinematics of mixing in granular flows. *Phys. Fluids* **23** (10), 103302.

Cisar, S. E., Umbanhowar, P. B. & Ottino, J. M. 2006 Radial granular segregation under chaotic flow in two-dimensional tumblers. *Phys. Rev. E* **74** (5).

Danckwerts, P. V. 1952 The definition and measurement of some characteristics of mixtures. *Appl. Sci. Res. A* **3** (4), 279–296.

Dolgunin, V. N. & Ukolov, A. A. 1995 Segregation modeling of particle rapid gravity flow. *Powder Technol.* **83** (2), 95–103.

Drahun, J. A. & Bridgwater, J. 1983 The mechanisms of free surface segregation. *Powder Technol.* **36**, 39–53.

Dury, C. M. & Ristow, G. H. 1997 Radial segregation in a two-dimensional rotating drum. *J. Phys. I* **7** (5), 737–745.

Dury, C. M. & Ristow, G. H. 1999 Competition of mixing and segregation in rotating cylinders. *Phys. Fluids* **11** (6), 1387–1394.

Fan, Y. & Hill, K. M. 2011 Theory for shear-induced segregation of dense granular mixtures. *New J. Phys.* **13**, 095009.

Fan, Y., Schlick, C. P., Umbanhowar, P. B., Ottino, J. M. & Lueptow, R. M. 2014*a* Modelling size segregation of granular materials: the roles of segregation, advection and diffusion. *J. Fluid Mech.* **741**, 252–279.

Fan, Y., Umbanhowar, P. B., Ottino, J. M. & Lueptow, R. M. 2013 Kinematics of monodisperse and bidisperse granular flows in quasi-two-dimensional bounded heaps. *Proc. R. Soc. A* **469**, 20130235.

Fan, Y., Umbanhowar, P. B., Ottino, J. M. & Lueptow, R. M. 2014*b* Shear-rate-independent collisional diffusion in granular materials. *Phys. Rev. Lett., under review* .

Fiedor, S. J. & Ottino, J. M. 2005 Mixing and segregation of granular matter: multi-lobe formation in time-periodic flows. *J. Fluid Mech.* **533**, 223–236.

Gray, J. M. N. T. & Ancey, C. 2009 Segregation, recirculation and deposition of coarse particles near two-dimensional avalanche fronts. *J. Fluid Mech.* **629**, 387–423.

Gray, J. M. N. T. & Ancey, C. 2011 Multi-component particle-size segregation in shallow granular avalanches. *J. Fluid Mech.* **678**, 535–588.

Gray, J. M. N. T. & Chugunov, V. A. 2006 Particle-size segregation and diffusive remixing in shallow granular avalanches. *J. Fluid Mech.* **569**, 365–398.

Gray, J. M. N. T. & Hutter, K. 1997 Pattern formation in granular avalanches. *Continuum Mech. Therm.* **9** (6), 341–345.

Gray, J. M. N. T., Shearer, M. & Thornton, A. R. 2006 Time-dependent solutions for particle-size segregation in shallow granular avalanches. *Proc. Roy. Soc. A* **462** (2067), 947–972.

Gray, J. M. N. T. & Thornton, A. R. 2005 A theory for particle size segregation in shallow granular free-surface flows. *Proc. R. Soc. A* **461**, 1447–1473.

Hill, K. M., Gioia, G. & Amaravadi, D. 2004 Radial segregation patterns in rotating granular mixtures: Waviness selection. *Phys. Rev. Lett.* **93** (22).

Hill, K. M., Khakhar, D. V., Gilchrist, J. F., McCarthy, J. J & Ottino, J. M. 1999 Segregation-driven organization in chaotic granular flows. *Proc. Nat. Acad. Sci.* **96**, 11701–11706.

Hutter, K, Svendsen, B & Rickenmann, D 1996 Debris flow modeling: A review. *Continuum Mech. Therm.* **8** (1), 1–35.

Jain, N., Ottino, J. M. & Lueptow, R. M. 2002 An experimental study of the flowing granular layer in a rotating tumbler. *Phys. Fluids* **14** (2), 572–582.

Jain, N., Ottino, J. M. & Lueptow, R. M. 2004 Effect of interstitial fluid on a granular flowing layer. *J. Fluid Mech.* **508**, 23–44.

Jain, N., Ottino, J. M. & Lueptow, R. M. 2005 Regimes of segregation and mixing in combined size and density granular systems: an experimental study. *Granul. Matter* **7** (2-3), 69–81.

Khakhar, D. V., Orpe, A. V. & Ottino, J. M. 2001 Continuum model of mixing and size segregation in a rotating cylinder: concentration-flow coupling and streak formation. *Powder Technol.* **116** (2-3), 232–245.

Makse, H. A. 1999 Continuous avalanche segregation of granular mixtures in thin rotating drums. *Phys. Rev. Lett.* **83** (16), 3186–3189.

Marks, B., Rognon, P. & Einav, I. 2012 Grainsize dynamics of polydisperse granular segregation down inclined planes. *J. Fluid Mech.* **690**, 499–511.

May, L. B. H., Golick, L. A., Phillips, K. C., Shearer, M. & Daniels, K. E. 2010 Shear-driven size segregation of granular materials: Modeling and experiment. *Phys. Rev. E* **81**, 051301.

Meier, S. W., Barreiro, D. A. M., Ottino, J. M. & Lueptow, R. M. 2008 Coarsening of granular segregation patterns in quasi-two-dimensional tumblers. *Nat. Phys.* **4** (3), 244–248.

Meier, S. W., Cisar, S. E., Lueptow, R. M. & Ottino, J. M. 2006 Capturing patterns and symmetries in chaotic granular flow. *Phys. Rev. E* **74** (3).

Meier, S. W., Lueptow, R. M. & Ottino, J. M. 2007 A dynamical systems approach to mixing and segregation of granular materials in tumblers. *Adv. Phys.* **56** (5), 757–827.

Mellmann, J. 2001 The transverse motion of solids in rotating cylinders - forms of motion and transition behavior. *Powder Technol.* **118** (3), 251–270.

Metcalfe, G. 1996 Experiments on mixing and segregating granular materials. In *Chemeca 96: Excellence in Chemical Engineering; 24th Australian and New Zealand Chemical Engineering Conference and Exhibition*, *National conference publication (Institution of Engineers, Australia)*, vol. 6, pp. 123–128.

Orpe, A. V. & Khakhar, D. V. 2001 Scaling relations for granular flow in quasi-two-dimensional rotating cylinders. *Phys. Rev. E* **64** (3).

Ottino, J. M. & Khakhar, D. V. 2000 Mixing and segregation of granular materials. *Annu. Rev. Fluid Mech.* **32**, 55–91.

Pereira, G. G. & Cleary, P. W. 2013 Radial segregation of multi-component granular media in a rotating tumbler. *Granul. Matter* **15** (6), 705–724.

Pignatel, F., Asselin, C., Krieger, L., Christov, I. C., Ottino, J. M. & Lueptow, R. M. 2012 Parameters and scalings for dry and immersed granular flowing layers in rotating tumblers. *Phys. Rev. E* **86** (1,1).

Prigozhin, L. & Kalman, H. 1998 Radial mixing and segregation of a binary mixture in a rotating drum: Model and experiment. *Phys. Rev. E* **57** (2, B), 2073–2080.

Savage, S. B. & Lun, C. K. K. 1988 Particle size segregation in inclined chute flow of dry cohesionless granular solids. *J. Fluid Mech.* **189**, 311–335.

Schlick, C. P., Christov, I. C., Umbanhowar, P. B., Ottino, J. M. & Lueptow, R. M. 2013 A mapping method for distributive mixing with diffusion: Interplay between chaos and diffusion in time-periodic sine flow. *Phys. Fluids* **25** (5), 052102.

Schlick, C. P., Fan, Y., Isner, A. B., Umbanhowar, P. B., Ottino, J. M. & Lueptow, R. M. 2014 Applying a model for segregation of bidisperse granular material to physical systems: The quasi-two-dimensional bounded heaps. *AIChE J., In preparation* .

Shearer, M., Gray, J. M. N. T. & Thornton, A. R. 2008 Stable solutions of a scalar conservation law for particle-size segregation in dense granular avalanches. *Eur. J. Appl. Math* **19** (1), 61–86.

Shinohara, K., Shoji, K. & Tanaka, T. 1972 Mechanism of size segregation of particles in filling a hopper. *Ind. Eng. Chem. Process Des. Dev.* **11**, 369–376.

Silbert, L. E., Grest, G. S., Brewster, R. & Levine, A. J. 2007 Rheology and contact lifetimes in dense granular flows. *Phys. Rev. Lett.* **99**, 068002.

Singh, M. K., Galaktionov, O. S., Meijer, H. E. H. & Anderson, P. D. 2009 A simplified approach to compute distribution matrices for the mapping method. *Comput. Chem. Eng.* **33** (8), 1354–1362.

Thornton, A. R. & Gray, J. M. N. T. 2008 Breaking size segregation waves and particle recirculation in granular avalanches. *J. Fluid Mech.* **596**, 261–284.

Tunuguntla, D. R., Bokhove, O. & Thornton, A. R. 2014 A mixture theory for size and density segregation in shallow granular free-surface flows. *J. Fluid Mech.* **749**, 99–112.

Williams, J. C 1968 The mixing of dry powders. *Powder Technol.* **2**, 13–20.

Woodhouse, M. J., Thornton, A. R., Johnson, C. G., Kokelaar, B. P. & Gray, J. M. N. T. 2012 Segregation-induced fingering instabilities in granular free-surface flows. *J. Fluid Mech.* **709**, 543–580.

Appendix A. Asymptotic analysis of I_d in tumbler flow for $\Lambda\mathrm{Pe}$ small

In figure 11, it was shown that $I_d \sim (\Lambda\mathrm{Pe})^2$ for $\Lambda\mathrm{Pe} < O(1)$. Here, this relationship is verified using an asymptotic analysis.

It was shown that, in the flowing layer for $\epsilon \ll 1$,

$$\pm \Lambda\mathrm{Pe}\frac{\partial}{\partial \tilde{z}}\left[c_i(1-c_i)\right] \approx \epsilon\frac{\partial^2 c_i}{\partial \tilde{z}^2}, \tag{A 1}$$

where the "+" sign is used for large particles and the "−" sign is used for small particles. In order to simplify the complex dynamics of tumbler flow, consider this simple one dimensional problem at $\tilde{x}=0$ and $-\epsilon < \tilde{z} < 0$. Defining $\tilde{z}' = \tilde{z}/\epsilon$ (so $-1 < \tilde{z}' < 0$) and applying no flux boundary conditions at $\tilde{z}'=-1$ and $\tilde{z}'=0$, equation (A 1) becomes

$$\pm \Lambda\mathrm{Pe} c_i(1-c_i) = \frac{\partial c_i}{\partial \tilde{z}'}. \tag{A 2}$$

Also, let

$$\int_{-1}^{0} c_i(\tilde{z}')d\tilde{z}' = \frac{1}{2}, \tag{A 3}$$

so that the average small and large particle concentrations are equal in the domain.

For $\Lambda\mathrm{Pe}=0$, $c_s = c_l = 0.5$ for $-1 \leqslant \tilde{z}' \leqslant 0$. For $\Lambda\mathrm{Pe} \ll 1$, expand c_i about 0.5:

$$c_i(\tilde{z}') \sim 0.5 + (\Lambda\mathrm{Pe})\xi_i(\tilde{z}') + \ldots . \tag{A 4}$$

Substituting this expression into equation (A 2) yields

$$\pm \Lambda\mathrm{Pe}\left[0.25 - (\Lambda\mathrm{Pe})^2\xi_i^2\right] + \ldots = (\Lambda\mathrm{Pe})\frac{\partial \xi_i}{\partial \tilde{z}'} + \ldots . \tag{A 5}$$

The $O(\Lambda\mathrm{Pe})$ equation is

$$O(\Lambda\mathrm{Pe}): \quad \pm 0.25 = \frac{\partial \xi_i}{\partial \tilde{z}'}. \tag{A 6}$$

Solving this gives $\xi_i = \pm 0.25\tilde{z}' + A_i$, where A_i is a constant. From equation (A 3), $A_i = \pm 1/8$, giving

$$\begin{aligned} c_l(\tilde{z}') &= 0.5 + (\Lambda\mathrm{Pe})\left(\frac{1}{8}+\frac{1}{4}\tilde{z}'\right) + O((\Lambda\mathrm{Pe})^2),\\ c_s(\tilde{z}') &= 0.5 - (\Lambda\mathrm{Pe})\left(\frac{1}{8}+\frac{1}{4}\tilde{z}'\right) + O((\Lambda\mathrm{Pe})^2). \end{aligned} \tag{A 7}$$

In this simplified problem, I_d can be defined as

$$I_d(c) = \frac{1}{\bar{c}(1-\bar{c})}\int_{-1}^{0}(c-\bar{c})^2 d\tilde{z}', \tag{A 8}$$

where $\bar{c}=0.5$. Substituting equation (A 7) into this expression yields

$$I_d(c_i) \sim (\Lambda\mathrm{Pe})^2, \tag{A 9}$$

which is the same scaling that was found in figure 11.